

## DESIGN OPTIMIZATION OF HIGH-PERFORMANCE ELECTRODYNAMIC ACTUATORS FOR USE IN A CRYOGENICALLY COOLED TELESCOPE

J.-N. Aubrun, K. R. Lorell, and K. P. Silveira\*

## INTRODUCTION

Substantial improvements in infrared sensor technology, the ability to design optics suitable for use at cryogenic temperatures, and the advent of Space Shuttle operations have spurred the development of the Shuttle Infrared Telescope Facility (SIRTF) [Ref. 1]. SIRTF, operating at cryogenic temperatures, will be flown as a shuttle-attached payload for missions up to 14 days. One of the unique advantages of a cooled infrared telescope observing above the earth's atmosphere is its ability to detect and measure extremely faint objects. This ability is further enhanced by using a technique called space chopping. Space chopping requires the telescope secondary mirror to execute a rapid back-and-forth motion in a pattern closely approximating a square wave. This motion, performed at frequencies between 10 and 40 Hz with amplitudes ranging from 5 to 45 arcminutes, permits a continuous comparison of an object-field containing background radiation only with a nearby field containing background radiation plus source radiation. By collecting data from both object fields and subtracting the resultant outputs, the signal-to-noise ratio of very weak sources is substantially improved.

The requirements placed on the secondary mirror actuation system by space chopping are especially difficult to meet. Ideally, of course, the mirror should execute a perfect square wave, exhibit no overshoot or jitter, and be able to operate over a wide range of frequencies and amplitudes. The actuators must be compact enough to fit behind the secondary mirror while developing sufficient force to rapidly accelerate and decelerate the mirror. In addition, the power to operate the actuators must be minimized because any heat dissipated inside the telescope must be removed by the cooling system, which has a limited capacity.

In the sections that follow, an analysis and optimization of a mirror-actuator system for large-exursion/high-frequency chopping is developed. The results of this analysis, combined with laboratory measurements of a prototype actuator operating at cryogenic temperatures, allow performance predictions to be made for a real system utilizing this technology.

## PERFORMANCE CRITERIA AND POTENTIAL ADVANTAGES OF ELECTRODYNAMIC ACTUATORS

The performance criteria for the SIRTF secondary mirror are as follows:

- 20 Hz, 90 percent duty cycle chop
- $\pm 24$  arcmin amplitude
- 1000 g-cm<sup>2</sup> mirror inertia
- Reactionless design
- Energy dissipation of <200 mW
- Actuator dimensions not to exceed secondary mirror envelope

These pose extremely challenging problems for the control system designer. The usual requirements of aerospace systems for small size, light weight, and low power are augmented by the need to generate forces on the order of 50 to 100 N in a time frame of only 200 to 600  $\mu$ s.

Electrodynamic actuators are differentiated from the electromagnetic variety (Ref. 2) by their lack of a fixed magnetic field (see Figs. 1 and 2). By using two coils to generate the interactive magnetic fields, electrodynamic actuators are

\*Lockheed Missiles & Space Company, Co., Palo Alto Research Laboratory, Palo Alto California.

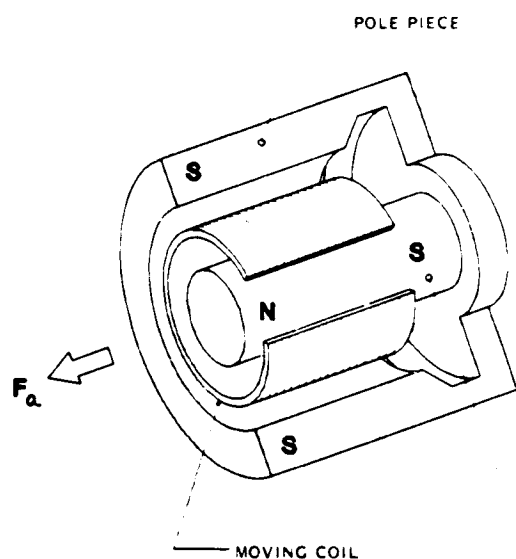


Fig. 1 Electromagnetic Actuator Cutaway View

ORIGINAL PAGE IS OF POOR QUALITY

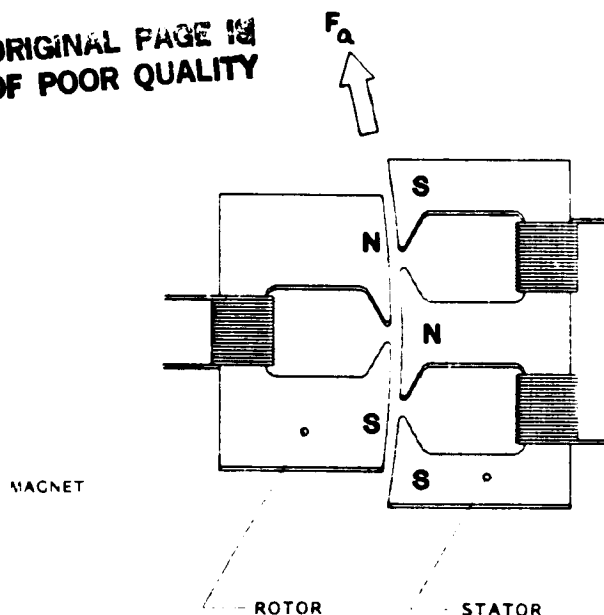


Fig. 2 Electrodynamic Actuator Detail Cutaway View

capable of delivering substantially more force than an electromagnetic device of comparable size. This is possible because higher flux concentrations can be obtained using electromagnets, very small gaps, and special core geometry and material to focus field effects.

Two characteristics of electrodynamic actuators, the comparatively large inertia of the moving portion and the additional power resulting from the use of two coils (rather than the single coil in an electro-magnetic machine) are potential disadvantages for the SIRTf application. Given the performance criteria, the questions to be answered are:

- Could any actuator, with physically realizable dimensions, produce the force required?
- What is the optimum actuator-linkage geometry, given the size and inertia-cancelling constraints on the mirror-actuator system?
- What is the predicted energy dissipation of the proposed design under SIRTf operation conditions?

#### DEVELOPMENT OF AN ANALYTICAL MODEL FOR ACTUATOR OPTIMIZATION

The relationship between the physical parameters used to describe the geometry of a generic mirror-actuator system are shown in Fig. 3. A real system would, of course, have two actuators to provide symmetric inertia cancellation. The analysis is somewhat simplified, however, by assuming the use of a single actuator.

The control system parameters  $\alpha$  and  $\beta$ , which affect the design of the actuator, are illustrated in Figs. 4 and 5. The ratio of the total transition time  $t_T$  to the time during which the actuator is used to apply a force  $t_A$  (for either acceleration or deceleration) is defined as  $\alpha$ . The duty cycle, or percentage of a total chop cycle during which the mirror is actually available to the optical system, is defined as  $\beta$ . Together  $\alpha$  and  $\beta$  represent important tradeoff parameters in both the design of the mirror-actuator system and the overall philosophy of the telescope system. Figure 5 demonstrates the impact on the actuator requirements of an 11 percent decrease in data-taking capability during a 20-Hz chop ( $\beta$  changed from 0.9 to

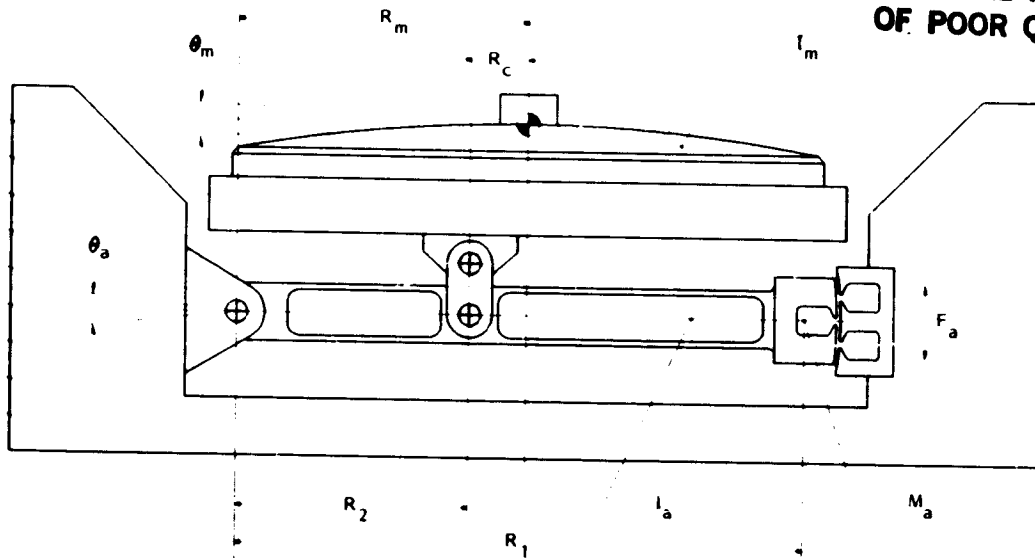


Fig. 3 Secondary Mirror Actuator

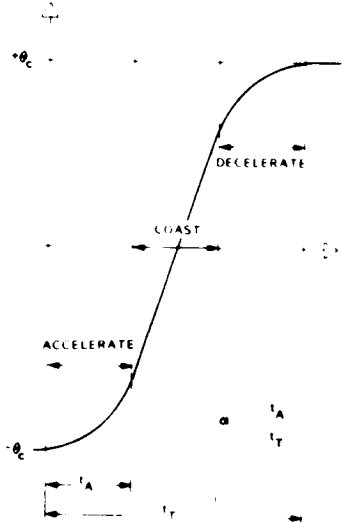


Fig. 4 Transition Period Detail

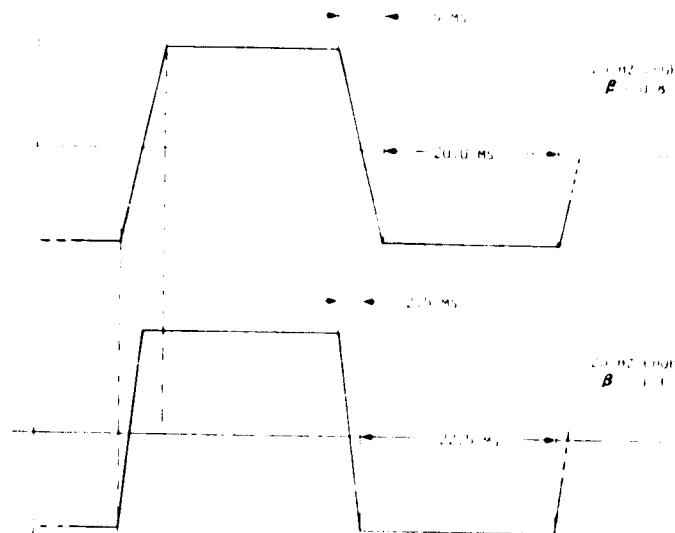


Fig. 5 Effect of Duty Cycle Variation

0.8). The force required to accelerate the mirror decreases by a factor of almost 10, thus placing substantially lower demands on actuator performance and power consumption.

Relations (1) through (8) were derived by analyzing the requirements for mirror acceleration/deceleration, inertia cancellation, and linkage geometry of the mirror and actuator system. Defining  $\theta_c$ ,  $\nu$ , and  $\gamma$  respectively as the mirror chopping amplitude, the chopping frequency, and the actuator gear ratio  $R_c/R_2$ , the following relations are found:

balancing condition: 
$$\gamma = I_m / (I_a + m_a R_1^2) \quad (1)$$

force required: 
$$f_r = (I_m + I_a + m_a R_1^2) C_\theta / R_1 \quad (2)$$

where

ORIGINAL PAGE IS  
OF POOR QUALITY

$$C_{\theta} \triangleq 4v^2 e_c / \alpha (1 - \alpha) (1 - \beta)^2 \quad (3)$$

force  
available:

$$f_a = (K_a / \delta_a) m_a \quad (4)$$

The quantity  $(K_a / \delta_a)$  is the ratio of the force developed per unit active area of the pole pieces to the mass per unit area of the pole pieces. The estimate of available actuator force modeled in Eq. (4) is a highly simplified approximation and is heavily dependent on core material and geometry.

The simultaneous solution of (2) and (4) requires that:

$$K_a / \delta_a > R_1 C_{\theta} \quad (5)$$

The actuator mass is then given by

$$m_a = \frac{(I_m + I_a) C_{\theta}}{R_1 (K_a / \delta_a - R_1 C_{\theta})} \quad (6)$$

Resistive losses in the actuator may be calculated from the basic relationship for energy dissipation in a resistor

$$E_R = \int_0^t R i^2 dt$$

This leads to the expression for the average power dissipated by a pulse-actuated system

$$P_E = \frac{8}{3} v R i_{\max}^2 t_A \quad (7)$$

Assuming that the resistance  $R$  is a function of the size of the pole piece (a larger pole piece will result in a longer winding and hence a higher resistance), then Eq. (7) may be written as

$$P_E = \frac{4}{3} R' m_a i_{\max}^2 \alpha (1 - \beta) \quad (8)$$

where  $R'$  is the resistance per unit mass of the pole piece.

The mechanical energy imparted to the mirror/actuator system can also be calculated as well as the resultant power. However, the value of the mechanical power (and hence the potential dissipation of energy) is several orders of magnitude less than the typical values obtained for electrical energy losses and so will not be considered here.

#### PARAMETRIC OPTIMIZATION OF ACTUATOR REQUIREMENTS

From Eq. (6) it can be seen that a minimum value for  $m_a$  (and thus for  $f_r$ ) will be achieved when

$$R_1 = (K_a / \delta_a) / 2C_{\theta} \quad (9)$$

The actuator mass will be in this case

$$m_a = 4(I_m + I_a) C_{\theta}^2 / (K_a / \delta_a)^2 \quad (10)$$

and thus the optimal gear ratio:

$$\gamma = \frac{I_m}{I_m + 2I_a} \quad (11)$$

ORIGINAL PAGE IS  
OF POOR QUALITY

Finally, the force required from the actuator is:

$$F_a = 4(I_m + I_a) C_\theta^2 / (K_a / \delta_a) \quad (12)$$

Equation (12) can be obtained either by substituting the value of  $m_a$  in (10) into the force available model in (4) or by substitution in (2) with  $R_1$  from (9). This is possible because we have assumed the force required  $f_r$  equal to the force available  $f_a$ .

Figures 6 and 7 display the results of calculations to determine actuator performance requirements as a function of the parameters  $\beta$  and  $K_a / \delta_a$ . In all of these calculations,  $\alpha = 0.33$ . This value minimizes the electrical power in (8) when  $m_a$  is provided by (10).

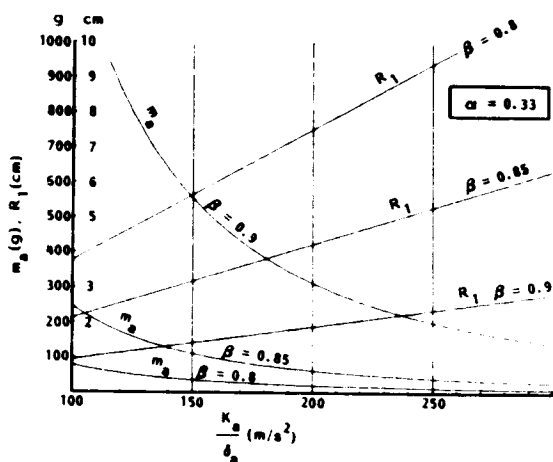


Fig. 6 Optimal Mass ( $m_a$ ) and Lever Arm ( $R_1$ ) Versus  $K_a / \delta_a$

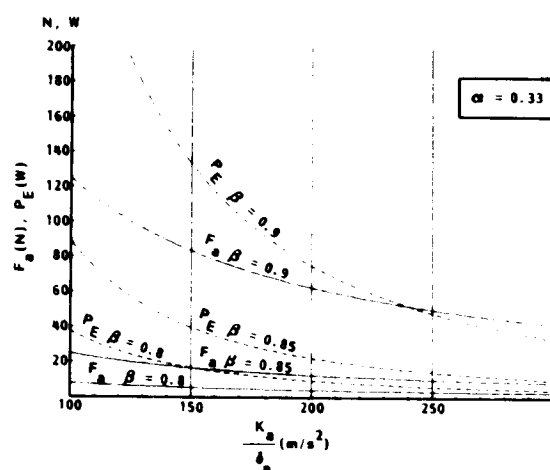


Fig. 7 Force Required ( $F_a$ ) and Power Dissipated ( $P_E$ ) Versus  $K_a / \delta_a$

Three values of  $K_a / \delta_a$ , 150, 200, and 250  $m/s^2$  have been highlighted in Figs. 6 and 7. These values represent the range of  $K_a / \delta_a$  to be expected from well designed electrodynamic actuators and thus illustrate the region from which design selections can be made for the dependent variables.

In Fig. 6 the changes in actuator pole-piece mass  $m_a$  and actuator arm length  $R_1$  are plotted versus  $K_a / \delta_a$  for three values of duty cycle  $\beta$ . It is clear from both sets of curves that to achieve a  $\beta = 0.9$  will require an actuator in the 250- $m/s^2$  class. A compromise design in which  $\beta = 0.85$  (slight degradation in chopping performance at 20 Hz) with  $K_a / \delta_a = 200 m/s^2$  indicates a required mass of 75 g at a radius of 4.2 cm.

In Fig. 7, the changes in required force  $F_a$  and dissipated electrical power  $P_E$  are shown as functions of  $K_a / \delta_a$ . The assumptions of  $\theta_c = 24$  arcmin,  $\nu = 20$  Hz, and  $R' = 60 \Omega/kg$  were made for these calculations. The difficulty of meeting the  $\beta = 0.9$  requirement is very apparent. Even for a state-of-the-art design, a force of 55 N dissipating 54 W would be required. For a more easily designed actuator with a  $K_a / \delta_a = 150 m/s^2$ , the required force and dissipated power are 85 N and 131 W respectively. These values are too large by a factor of 3. The improvement obtained by

setting  $\beta = 0.85$  is dramatic, assuming a  $200\text{-m/s}^2$  design. The power dissipated drops to 25 W while  $m_a = 70$  g and  $F_a = 17$  N.

## ACTUATOR EXPERIMENT VALIDATION

Preliminary laboratory experiments were conducted [Ref. 3] to validate the concepts and design of the SIRTf secondary mirror and its actuator(s). Tests were conducted on the actuator to verify force levels and power consumption at ordinary and cryogenic temperatures. The electrodynamic actuator chosen for the test had not been specially optimized; thus the actual performance is below the SIRTf requirements. However, the results are readily scalable to an actual SIRTf design and sufficient to demonstrate feasibility. Moreover, the techniques developed for these tests, particularly at cryogenic temperatures, constitute a solid basis for designing future tests of the fully actuated secondary mirror.

## MEASUREMENT PRINCIPLES

### Force Measurements

Force measurements are made using a technique similar to that of the ballistic pendulum. This particular method has two advantages: first, the actuator is operating in a mode similar to the actual mode and, second, it is simple to implement and accurate results can be obtained. A short current pulse (200 to 1200  $\mu\text{s}$ ) is sent to the actuator coils, communicating a certain amount of kinetic energy to the system, which gradually loads up the spring system constituted by the pivot and the gravity field. The maximum amplitude deflection  $\theta_{\text{max}}$  is thus a measure of the force applied to the actuator. To quantify these principles, the dynamic model shown in Fig. 8 is used. The actuator is mounted vertically, with its CG below the flex pivot, and the equations of motion are given by:

$$I\ddot{\theta} + (k + Mga)\theta = Fr \quad (13)$$

where  $I$  is the actuator inertia about the pivot,  $k$  is the pivot spring constant,  $M$  is the total mass of the moving part,  $a$  is the position of the center of mass,  $g$  is the acceleration due to gravity,  $F$  is the electrodynamic force generated between the pole pieces at a distance  $r$  from the pivot, and  $\theta$  is the deflection angle.

For a pulse of short duration  $\Delta t$ , it can be shown that the average force  $F$  is:

$$F = (\theta_{\text{max}} / r\Delta t) \sqrt{I(k + Mga)} \quad (14)$$

The quantities  $I$  and  $k + Mga$  are first derived from the measured natural frequencies of oscillation of the actuator in the following cases: (1) nominal position, and (2) nominal position with added mass  $m$  at distance  $d$  from the pivot.

### Actuator Force Coefficient

The force produced by the electrodynamic actuator is directly proportional to the product of the currents in the rotor ( $i_1$ ) and stator ( $i_2$ ) coils:

$$F = k_f i_1 i_2 \quad (15)$$

where the coefficient  $k_f$  is expressed in Newtons per square Ampere. Because of the coil inductance, saturation of the power amplifiers driving the coils, and other nonlinearities, the pulse shapes are usually not square, especially for short durations. The measurements give an average value of  $F\Delta t$ , and the force coefficient is determined by the formula:

$$k_F = (F\Delta t) / \int_0^{\Delta t} i_1 i_2 dt \quad (16)$$

In these studies, the maximum achievable  $F$  is more important for the design than the actual value of  $k_F$ , but linear and saturation ranges must be assessed for scalability and extrapolation to different designs.

Power Measurement Principle

The electrical power dissipated in the actuator is of primary concern for the SIRTf design, and accurate measurement is essential. The method chosen here is purely electrical. A general circuit model for one of the actuator coils is shown in Fig. 9. The main constituents of this circuit are the inductance  $L$ , the resistance  $R$ , and an induction voltage  $e$ , which includes the interactions of the coil with the other part of the actuator and other kinds of losses.

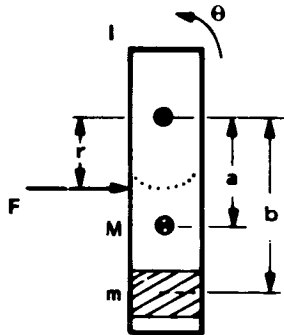


Fig. 8 Dynamic Model

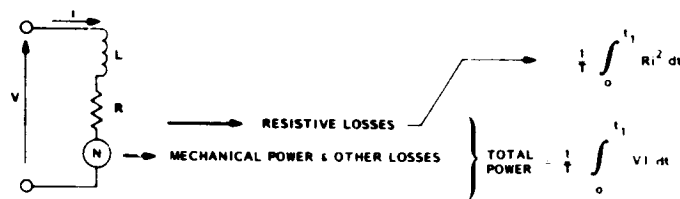


Fig. 9 Power Measurement

Measuring the input voltage  $V$  and current  $i$  in the coils leads to an evaluation of the total energy fed to the system during the interval  $\Delta t$ ,

$$E_T = \sum_k \int_0^{\Delta t} V_k i_k dt \quad k = 1, 2 \quad (17)$$

The resistive losses are obtained by

$$E_R = \sum_k \int_0^{\Delta t} R_k i_k^2 dt, \quad (18)$$

$$E_m = F\bar{\Delta t} = k_F \int_0^{\Delta t} i_1 i_2 dt \quad (19)$$

The energy balance requires that

$$E_T = E_m + E_R + E_\theta \quad (20)$$

where  $E_\theta$  represents non-resistive losses. It is thus seen that measurements of  $V$ ,  $i$ , and  $R$  can be used to determine the energy losses in the actuator and thus the heat generated.

As shown previously, since the pulse shapes are not square it is necessary to perform an actual integration over some period of time at during which there is electrical activity present in the system. (This time may in fact significantly exceed the original pulse width of the input to the power amplifiers.) Thus, each value determined for  $E_T$ ,  $E_R$ , etc., represents the energy per pulse, and the average power is then calculated by multiplying these values by the number of pulses per second.

### DATA ACQUISITION AND PROCESSING

The actuator dynamic characterization and the force and power measurements were performed using a sophisticated digital data acquisition and processing system involving an STI/DEC 11-23 microprocessor, A/D and DAC interfaces, a separate digital frequency generator, a pulse generator and power amplifiers, and a data analysis software package (VAMP). This system is used in two different modes (Fig. 10):

- (1) A slow mode in which the actuator is pulsed every 5 or 10 s and the data are taken at a 200-Hz sampling rate.
- (2) A fast mode in which the actuator is pulsed at a 200.1-Hz rate by an independent frequency generator triggering the pulse generator. The 11-23 is still taking data at 200 Hz and, because of the slight difference in frequencies, the equivalent (or virtual) sampling time is about 2.5  $\mu$ s.

### CRYOGENIC MEASUREMENTS SETUP

These measurements are made using a helium dewar as shown in Fig. 11. A small window allows a laser beam to be reflected from a mirror attached to the actuator. The reflected beam is detected by a linear photosensor whose output is thus proportional to the actuator rotation angle  $\theta$ . The current into and voltage across the coils are picked up outside of the dewar, near the connector. Thermistors are glued to various parts of the actuator and internal fixtures to determine the local temperatures. Power data are acquired in a short burst to minimize heat dissipation, which would otherwise be significant for 200-Hz operations. Because of the short time available at low temperature due to the limited capacity and insulation of the dewar, all the various measurements are stored in memory to be processed and studied later.

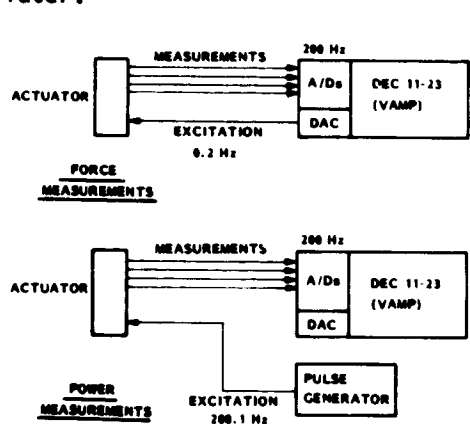


Fig. 10 Data Acquisition and Processing System

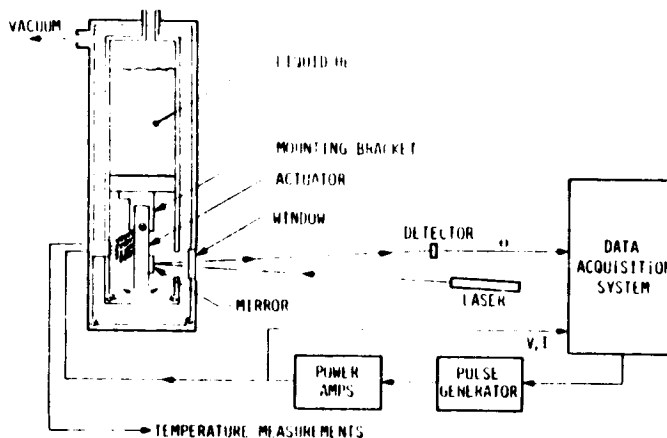


Fig. 11 Cryogenic Measurements Variation

### EXPERIMENTAL RESULTS

Data were taken at ordinary temperature and at temperatures around 16 K. In both cases the actuator was installed inside the dewar, except for preliminary measurements of mass/inertia properties.

ORIGINAL DESIGN  
OF POOR QUALITY

Mass/Inertia Properties

The actuator under test was found to have the following characteristics:

$$k = 0.69 \text{ N-m/rad} \quad Mga = 2.95 \times 10^{-2} \text{ N-m/rad} \quad I = 1.60 \times 10^{-4} \text{ kg-m}^2$$

The value of  $r$  (application point of the electrodynamic force) is 0.0212 m.

Force Measurements

These measurements were taken for commanded pulse lengths of 400, 600, and 1200  $\mu\text{s}$  at room temperature and at 500 and 600  $\mu\text{s}$  at cryogenic temperatures. A typical data set for the cryogenic runs is shown in Fig. 12. Values for the actuator force coefficient were found to be in the range of 0.3 to 0.6  $\text{N/A}^2$ . Fig. 13 plots the relationship between the calculated values and those measured experimentally. The assumption of  $Ka/\delta_a = 100 \text{ m/s}^2$  for this actuator appears to be substantially correct based on the fidelity of the computed values in Fig. 13.

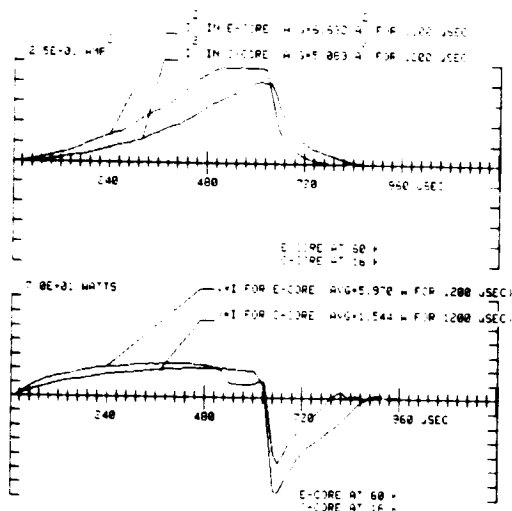


Fig. 12 Total Input Power (VI) and Resistive Losses ( $i^2$ ) at Cryogenic Temperatures

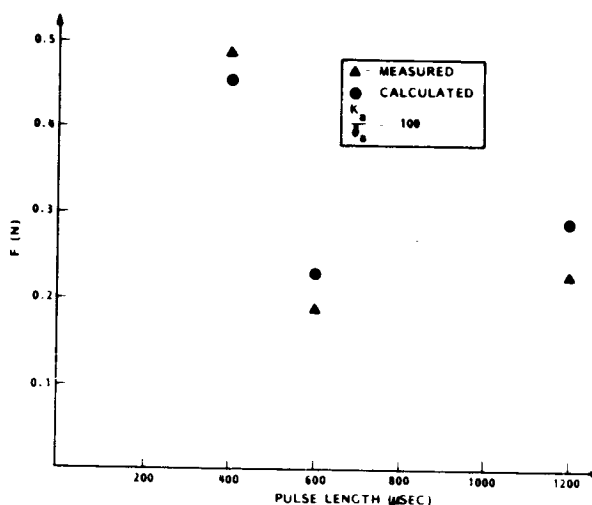


Fig. 13 Actuator Force for Various Pulse Lengths

Power Measurements

Data were taken with the actuator cooled to below  $\text{LN}_2$  temperature (E-core at 60 K and C-core at 16 K). The results of these tests are summarized in Table 1:

Table 1 POWER DISSIPATION

Pulse Length ( $\mu\text{s}$ )	Average Total Power (W) Per 1200 $\mu\text{s}$		Average $i^2$ ( $\text{A}^2$ ) Per 1200 $\mu\text{s}$	
	C-Core	E-Core	C-Core	E-Core
500	2.785	4.653	3.541	4.886
600	1.544	5.970	5.083	6.692

Measurements of the C-core and E-core winding resistance indicated a drop of approximately a factor of 10 from room temperature values. However a factor of 100

to 150 was expected at 16 K (Ref. 4). To verify the assumption of greatly increased conductivity, a separate test was conducted in which the complete E- and C-cores of a disassembled PPM actuator were cooled directly in an LHe bath until they stabilized at 4.2 K. These data, summarized in Table 2, support the claim that substantially lowered resistivity will occur at SIRTf secondary mirror operating temperatures, even without the use of high-purity, annealed copper wire.

Data from Tables 1 and 2 and Fig. 12 may now be combined to show force generated and the associated energy dissipation (Table 3).

Table 2 RESISTIVITY

ORIGINAL PAGE IS  
OF POOR QUALITY

Temperature (K)	E-Core Resistance (ohms)	C-Core Resistance (ohms)	Average Reduction
Room Ambient	1.935	1.660	---
77	0.220	0.203	8.5
4.2	0.017	0.013	120.0

Table 3 GENERATED FORCE AND ENERGY LOSS

Commanded Pulse Length ( $\mu$ s)	Force Generated (N)	Total $i^2R$ Energy Loss (E+C Cores) per Pulse (J)
500	2.91	$1.55 \times 10^{-4}$
600	3.32	$2.16 \times 10^{-4}$

Predicted Performance for SIRTf Actuators

Since both the force  $F$  generated by this type of actuator and the resistive losses are a function of  $i^2$ , the average power dissipation  $P_{ave}$  is thus proportional to  $F$ . This scaling relation was used with data from Table 3 to obtain the results in Table 4. Note that even at a 90 percent duty cycle, total power dissipation is less than 150 mW.

Table 4 POWER DISSIPATION

Duty Cycle (500 $\mu$ /s Pulse)	Force Level Required (20 Hz at 45 arcmin amplitude) (N)	Average Power Dissipated by Resistive Losses $K_a/\delta_a = 200 \text{ ms}^2$ (W)
$\beta = 0.85$ (85 percent) $\alpha = 0.33$	17	0.036
$\beta = 0.90$ (90 percent) $\alpha = 0.33$	65	0.132

#### REFERENCES

1. F. C. Witleborn, and L. S. Young, "A Cooled Infrared Telescope for the Space Shuttle - the Shuttle Infrared Telescope Facility (SIRTF)," AIAA Paper 76-174, 21st Annual Meeting of the American Astronautical Society, Denver, 1975.
2. K. R. Lorell, R. R. Clappier, W. F. Barrows, and G. K. Lee, "A Microprocessor-Based Position Control System for a Telescope Secondary Mirror," Proceedings of the Joint IFAC/ESA Symposium on Automatic Control in Space, Noordwykerhout, The Netherlands, 1982.
3. Final Report LMSC-D877125, "Study of SIRTF Long-Life Feasibility," 1982.
4. K. D. Timmerhaus, et al., "Advances in Cryogen Engineering," p. 157, Plenum Press, Inc., New York, 1960.